HAL open science

Probing Low-Frequency Charge Noise in Few-Electron CMOS Quantum Dots

Cameron Spence, Bruna Cardoso Paz, Vincent Michal, Emmanuel Chanrion, David J Niegemann, Baptiste Jadot, Pierre-André Mortemousque, Bernhard Klemt, Vivien Thiney, Benoit Bertrand, et al.

To cite this version:

Cameron Spence, Bruna Cardoso Paz, Vincent Michal, Emmanuel Chanrion, David J Niegemann, et al.. Probing Low-Frequency Charge Noise in Few-Electron CMOS Quantum Dots. Physical Review Applied, 2023, 19 (4), pp.044010. 10.1103/PhysRevApplied.19.044010 . hal-04062049

HAL Id: hal-04062049

https://hal.science/hal-04062049v1

Submitted on 25 Aug 2023

HAL is a multi-disciplinary open access archive for the deposit and dissemination of scientific research documents, whether they are published or not. The documents may come from teaching and research institutions in France or abroad, or from public or private research centers.

L'archive ouverte pluridisciplinaire **HAL**, est destinée au dépôt et à la diffusion de documents scientifiques de niveau recherche, publiés ou non, émanant des établissements d'enseignement et de recherche français ou étrangers, des laboratoires publics ou privés.

Probing Low-Frequency Charge Noise in Few-Electron CMOS Quantum Dots

Cameron Spence,[1,*] Bruna Cardoso Paz,[1] Vincent Michal,[2] Emmanuel Chanrion,[1] David J. Niegemann,[1] Baptiste Jadot,[3] Pierre-André Mortemousque,[3] Bernhard Klemt,[1] Vivien Thiney,[1] Benoit Bertrand,[3] Louis Hutin,[3] Christopher Bäuerle,[1] Maud Vinet,[3] Yann-Michel Niquet,[2] Tristan Meunier,[1] and Matias Urdampilleta[1,†]

[1] *University Grenoble Alpes, CNRS, Grenoble INP, Institut Néel, Grenoble 38402, France*
[2] *University Grenoble Alpes, CEA, IRIG, Grenoble 38000, France*
[3] *University Grenoble Alpes, CEA, Leti, Grenoble F-38000, France*

(Received 20 September 2022; revised 21 December 2022; accepted 16 March 2023; published 4 April 2023)

Charge noise is one of the main sources of environmental decoherence for spin qubits in silicon, presenting a major obstacle in the path towards highly scalable and reproducible qubit fabrication. Here we demonstrate in-depth characterization of the charge noise environment experienced by a quantum dot in a CMOS-fabricated silicon nanowire. We probe the charge noise for different quantum dot configurations, finding that it is possible to tune the charge noise over two orders of magnitude, ranging from 1 $\mu\mathrm{eV}^2/\mathrm{Hz}$ to 100 $\mu\mathrm{eV}^2/\mathrm{Hz}$. In particular, we show that the top interface and the reservoirs are the main sources of charge noise, and their effect can be mitigated by controlling the quantum dot extension. Additionally, we demonstrate a method for the measurement of the charge noise experienced by a quantum dot in the few-electron regime. We measure a comparatively high charge noise value of 40 $\mu\mathrm{eV}^2/\mathrm{Hz}$ at the first electron, and demonstrate that the charge noise is highly dependent on the electron occupancy of the quantum dot.

DOI: 10.1103/PhysRevApplied.19.044010

I. INTRODUCTION

Spin qubits in silicon are a strong potential candidate for the eventual qubit of a scalable quantum computer [1]. State-of-the-art research has demonstrated long spin-coherence times [2], single-qubit gate fidelity above 99.9% [3], and two-gate fidelity over 99% [4] in silicon quantum dots. However, the coherence time of silicon qubits can be limited by combined natural or induced spin-orbit coupling and low-frequency $1/f$ charge noise [3,5]. This charge noise, induced by local electric field fluctuations, is a characteristic of the material and architecture used to form the qubit. In semiconductor devices, it is believed to be dominated by bistable charge traps, also called two-level systems (TLSs), in particular dangling bonds at the semiconductor/oxide interface or dopants in the active regions [6]. Quantum dots in silicon are tightly confined by material interfaces and therefore sensitive to charge noise [7].

Spin measurement and manipulation techniques have been shown to be compatible with industrially produced 300-mm- technology silicon nanowire devices [8–12]. However, these device geometries and fabrication processes are different from heterostructure-based devices. In particular, the lateral confinement is obtained by nanowire etching which could lead to an extra source of charge noise on the side walls. Moreover, the nanowire part which separates the quantum dots and the reservoirs is covered by the so-called SiN spacers, which is known to be a source of charge noise. Understanding the origin of charge noise is particularly relevant in the few-electron regime where the quantum dots are more sensitive to Coulomb disorder, and direct characterization of charge noise can be challenging. Therefore, characterizing the charge noise is important to direct fabrication and develop methods to mitigate its effect on qubits [13].

In this letter, we present the extended characterization of CMOS quantum dots fabricated on a foundry-compatible 300-mm wafer. In particular, we first show how we can probe the different sources of noise by modifying the electronic wave function. We find that the level of charge noise depends drastically on shape and position of the quantum dot within the channel. In the second part, we introduce a method to extract charge noise and its power spectral density at the single-electron level. This last result is of particular importance to understanding the role of charge noise in few-electron quantum dots, which is the relevant regime to operate as spin qubits. It enables simple measurements of the fluctuation in chemical potential, which is traditionally extracted via more complex experiments [3,14,15].

*cameron.spence@neel.cnrs.fr
†matias.urdampilleta@neel.cnrs.fr

 © 2023 American Physical Society

II. DEVICE DESIGN AND OPERATION

The device under study is a split-gate nanowire CMOS design fabricated on a foundry-compatible 300-mm wafer [16], identical to that shown in Fig. 1(a). The device design involves a semiconducting silicon channel which is covered by two parallel electrostatic plunger gates, marked G_1 and G_2. The channel has a width of 100 nm, a gate length of 60 nm, and a vertical split of 60 nm. The plunger gates are insulated from the channel by a resistive layer of native oxide and titanium nitride with a thickness of a few nanometers, marked in red in Fig. 1(b). The source and drain reservoirs are formed by high-density implantation of dopants in the areas of the channel not covered by the silicon nitride spacers (indicated in pink). A homogeneous back gate is formed by the silicon bulk below the buried oxide. In order to operate it as a gate at low temperature, an LED is used to generate charge carriers in the substrate. Once polarized, the voltage on the gate remains stable and the LED can be switched off. At higher temperatures, above 1 K, the back gate may be polarized without the use of the LED. Tests in the same configuration with and without the LED indicate that photoexcitation does not significantly contribute to the charge noise. In addition, a metal top gate is deposited above the plunger gates for finer control of the electrostatic environment of the channel.

The device has been measured in a ^{3}He refrigerator, with a base temperature of 300 mK. At this temperature, a quantum dot is formed under each front gate, G_1 and G_2. Additionally, the spatial extension and coupling to reservoirs of the quantum dots can be further tuned by applying voltage on the top gate and on the back gate [see Fig. 1(b)]. The identification of the number of electrons in each dot is achieved by operating one of the two quantum dots as a charge sensor. Figure 1(c) shows the stability diagram of V_{G1}, V_{G2}, which indicates the number of electrons in QD_1, using QD_2 as a charge sensor.

Charge noise measurements are performed by recording the source = drain current flowing through QD_1 as a

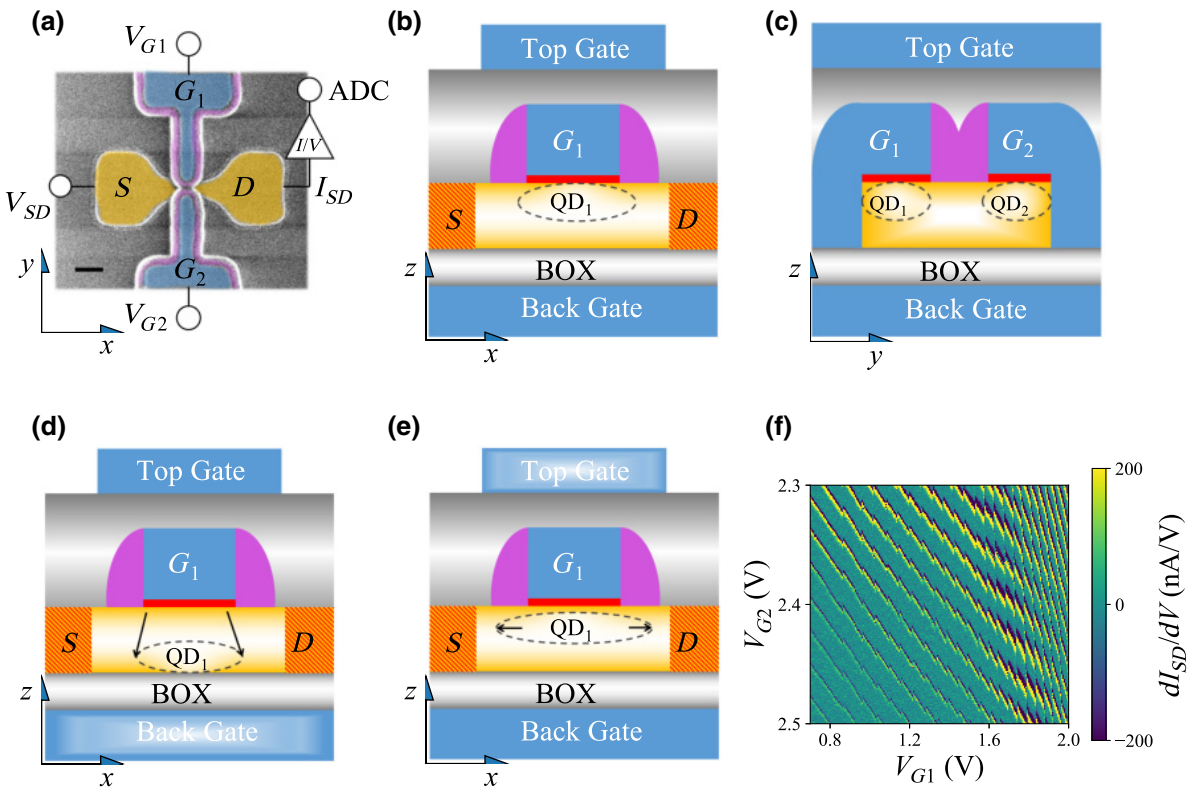

FIG. 1. (a) False-color SEM image of a CMOS nanowire identical to the one used to form quantum dots. The nanowire channel (yellow) is enveloped by electrostatic gates (blue), which are separated by nitride spacers (pink). The spacers screen the channel from the high-density doping used to define the source and drain. Measurements are performed by applying a bias voltage (V_{SD}) on the source contact and measuring the drain current (I_{SD}) at the drain contact via an I/V converter. The scale bar is 100 nm. (b) Cross-sectional schematic (not to scale) of the device parallel to the nanowire axis in (a). (c) Cross-sectional schematic (not to scale) of the device perpendicular to the nanowire axis in (a). (d) Depiction of the deformation of the quantum dot (QD_1) as the back gate voltage is increased. (e) Depiction of the deformation of the quantum dot (QD_1) as the top gate voltage is increased. (f) Two-dimensional stability diagram demonstrating charge sensing down to the first electron under G_2. The sharp cuts in the conductance peaks indicate the capacitive shift induced by the addition of an electron in the dot under G_2.

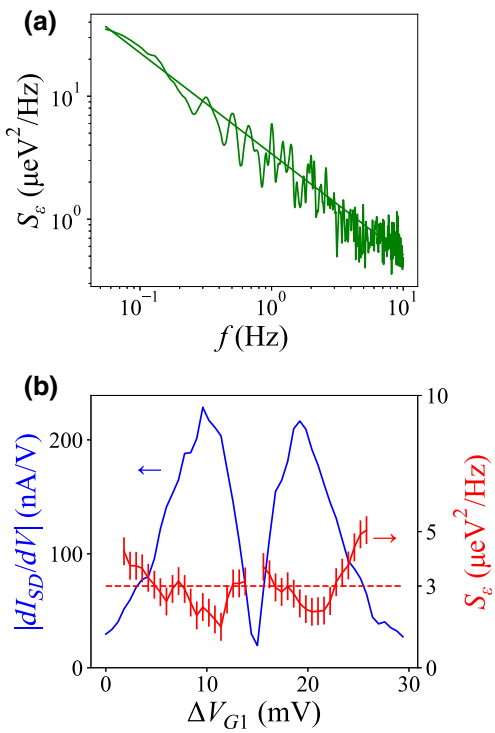

FIG. 2. (a) $1/f$-like power density spectrum acquired via Fourier transform of a current time trace, measured on the slope of a Coulomb peak. (b) Method for extracting the average charge noise value across a Coulomb peak. Current time traces are measured for varying values of V_{G1} across a Coulomb peak. The shape of the Coulomb peak is extracted from the average current value for each noise trace. The absolute conductance of the peak (blue) gives the sensitivity of the detector dot for each value of gate voltage. This is used to renormalize the power spectral density (PSD) measured at each gate voltage value. Spectra where the conductance is below 50 nS are discarded due to low sensitivity and overrenormalization leading to skewed results. The magnitude of the PSD at 1 Hz is extracted from a fit of the noise spectrum at acquisition points spanning the Coulomb peak (red). The average charge noise value for this measurement is indicated by the dashed line at 3 μeV^2/Hz.

function of time; this will be referred as the I_{SD} method latter on. A Fourier transform of the time trace gives the power spectral density (PSD) of the signal. The current noise spectrum is then renormalized by dI/dV_G and the lever arm α to account for the sensitivity of the detector at the measurement point. We can then plot the charge noise S_ϵ as a function of frequency [see Fig. 2(a)]. Figure 2(b) shows that the extracted charge noise at 1 Hz does not vary much over a Coulomb peak. The average value is close to 3 μeV^2/Hz at 360 mK, which is a relatively low value for silicon compared to other values obtained in literature [15,17–19]. We attribute the fluctuations across the Coulomb peak to the influence of gate G_1 on the electrostatic environment of the quantum dot (namely the TLS).

III. PROBING THE NOISE SOURCES IN THE MANY-ELECTRON REGIME

One of the main challenges when assessing the noise environment is disentangling the different sources of noise [20,21]. In a device where the accumulation interface is expected to be the dominant source of noise, it is important to distinguish it from other contributions such as noise originating from the core of the nanowire, reservoirs, or other interfaces. For this purpose, we can distort the quantum dot confinement potential in order to probe the spatial dependence of charge noise on a nanometer scale.

We start by studying the effect of the back gate which allows us to move QD_1 vertically within the channel. By applying a positive voltage on the back gate, the quantum dot which was originally confined against the top interface now moves towards the back interface. This is visible in Fig. 3(d), where the front gate G_1 to QD_1 capacitance is plotted as a function of the back gate. In parallel, we record the evolution of charge noise with back gate voltage [see Fig. 3(c)]. We observe that charge noise decreases as the quantum dot is less confined against the top interface. This is in good agreement with the literature which reports a large density of charge traps at the Si/SiO_2 gate interface [22,23]. It is also in qualitative agreement with the simulation of the effect of a single TLS above the interface on

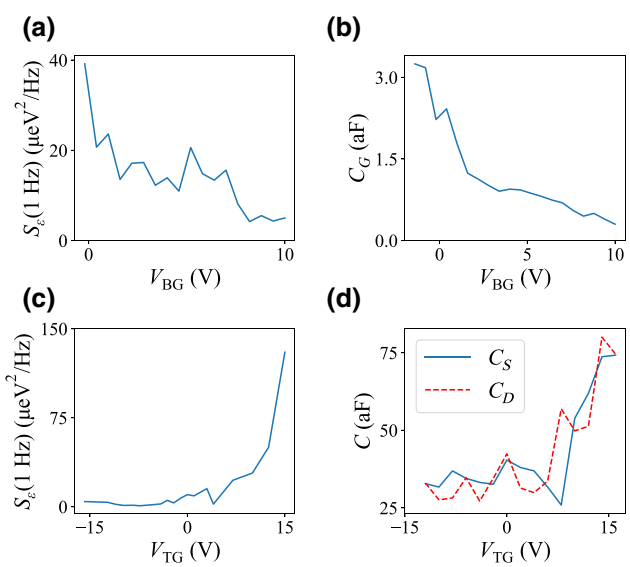

FIG. 3. (a) Power spectral density at 1 Hz measured as a function of the back gate voltage. The number of electrons in the dot remains fixed. (b) Variation in the plunger gate capacitance as a function of the back gate voltage. A lower capacitance indicates a weaker coupling to the plunger gate as the quantum dot moves vertically in the channel. (c) Power spectral density value at 1 Hz as a function of the top gate voltage. The number of electrons in the dot is constant for all values of V_{TG}. (d) Variation in the reservoir capacitances to the quantum dot as the top gate voltage is varied, measured simultaneously with the PSD in (c).

the chemical potential of the quantum dot as a function of back gate voltage (see Appendix A).

The reservoirs provide electrons to the quantum dot, but can also be a source of charge noise due to slowly varying fluctuators at the diffuse boundary. To investigate the effect of the reservoirs, we first bias the back gate in a region of relatively weak charge noise ($V_{\mathrm{BG}} = 10$ V). We then use the very top gate to extend the QD_1 wave function towards the reservoirs, while accounting for unwanted vertical extension by applying a compensating voltage on the plunger gate. Figures 3(a) and 3(b) present the evolution of the charge noise and of the source and drain capacitance, respectively, as a function of the top gate voltage. They show that as the capacitive coupling to reservoirs increases, the charge noise experienced by the quantum dot likewise increases in magnitude. Therefore, the reservoirs can also become the dominant source of noise either by directly modifying the chemical potential of the quantum dot or by modifying the tunnel barrier transparency. The main source of noise in the reservoirs is expected to be dopants that have diffused inside the tunnel junction, where the reservoirs stop being metallic. Another potential source of charge noise is the material deposited above this junction [the SiN spacers in pink in Fig. 1(e)] which has a nominally high density of TLS compared to SiO_2.

IV. CHARGE NOISE AT THE SINGLE-ELECTRON LEVEL

The charge noise of quantum dots is generally measured in the many-electron regime due to the simplicity of the I_{SD} measurement method [3]. However, spin qubits typically operate with few electrons. In this configuration, the environment of the device can be significantly different. The charge noise magnitude measured in the many-electron regime is therefore of limited value in determining the charge noise a qubit would experience. To illustrate the dramatic dependence on the number of localized electrons, we have observed a drastic reduction of charge noise when the number of electrons trapped in the QD_1 is increased from 10 to 30 [see Appendix B Fig. 7(a)]. The mechanism behind the reduction of the effect of charge noise is expected to be a combination of electric field screening due to the additional charges within the quantum dot, and an increase in the self-capacitance of the quantum dot through the geometric deformation of expansion.

The evaluation of charge noise in the single-electron regime is usually done by measuring the dephasing rate of the spin when limited by charge noise. This method requires coherent manipulation and readout of spins, which is complex to implement for large-scale characterization, and cannot readily be achieved, for example, at probe station temperatures. We propose here a simpler method which allows measurement of the charge noise at the single-electron level. The method consists of probing single-electron tunneling in real time, and investigating fluctuations in the tunnel rate and average dot occupancy. We start by setting the chemical potential of the single electron in resonance with the Fermi sea [see Fig. 4(a)] and digitizing tunneling events by charge sensing. We choose a regime of sensor operation where the step size between the two charge states is strong enough to be immune from charge noise effect on the sensor itself. We can then observe real-time tunneling in Fig. 4(b). By counting the number of tunneling events observed per second, we measure the equivalent current, $e\Gamma$ [see Fig. 4(c)]. Figure 4 (d) shows the corresponding noise spectrum after a Fourier transformation of the time trace and renormalization by the differential conductance. This plot corresponds to the optimal configuration of back gate and top gate voltages ($V_{\mathrm{BG}} \approx 10$ V, $V_{\mathrm{TG}} \approx 0$ V), which can reduce the charge noise at 1 Hz to around 1 $\mu\mathrm{eV}^2/\mathrm{Hz}$ (extrapolated from the fit). The differential conductance is obtained by measuring $e\Gamma$ while scanning the gate G_1. This leads to a Coulomb peak whose derivative is plotted in Fig. 4(e) (blue curve). On the same figure, we have extracted the charge noise at 1 Hz across the Coulomb peak for a typical configuration ($V_{\mathrm{BG}}, V_{\mathrm{TG}} \approx 0$ V), which leads to an average value of 40 $\mu\mathrm{eV}^2/\mathrm{Hz}$, an order-of-magnitude-higher noise compared to the many-electron regime [Fig. 2(b)]. As in the many-electron regime, the charge noise is extremely dependent on the biasing conditions.

So far, the extraction of charge noise in both the many- and few-electron regimes, using the I_{SD} and the $e\Gamma$ methods respectively, has not disentangled the contributions of tunnel barrier fluctuations and chemical potential fluctuations to the charge noise. We now try to extract the charge noise purely acting on the chemical potential by probing the mean occupancy of the quantum dot, $\langle N \rangle$.

$\langle N \rangle$ is extracted by averaging the real-time measurements using the expression $\langle N \rangle = \langle \tau_{N=1} \rangle / (\langle \tau_{N=1} \rangle + \langle \tau_{N=0} \rangle)$, where $\langle \tau_{N=1} \rangle$ and $\langle \tau_{N=0} \rangle$ are the average times during which the dot has one or zero electron, which correspond respectively to the time spent above or below threshold in Fig. 4(b). To build the PSD of the charge occupancy, the quantity $\langle N \rangle$ is measured as a function of time and Fourier-transformed. Further renormalization using $d\langle N \rangle / dV_G$ leads to the charge noise on chemical potential only [see Fig. 4(f)]. We obtain an average charge noise power of 20 $\mu\mathrm{eV}^2/\mathrm{Hz}$. This value is smaller than that obtained from tunneling rate extraction. This discrepancy is likely explained by accounting for charge noise in the tunnel barrier. To extract this latter parameter, we would need a gate to control and extract the quantum dot sensitivity to tunnel coupling.

To further explore the dependence of the charge noise on the number of electrons, we conduct similar measurements for the second and third electrons, which are presented in Fig. 5 together with other points measured using the I_{SD} method. The error bars in the few-electron regime are

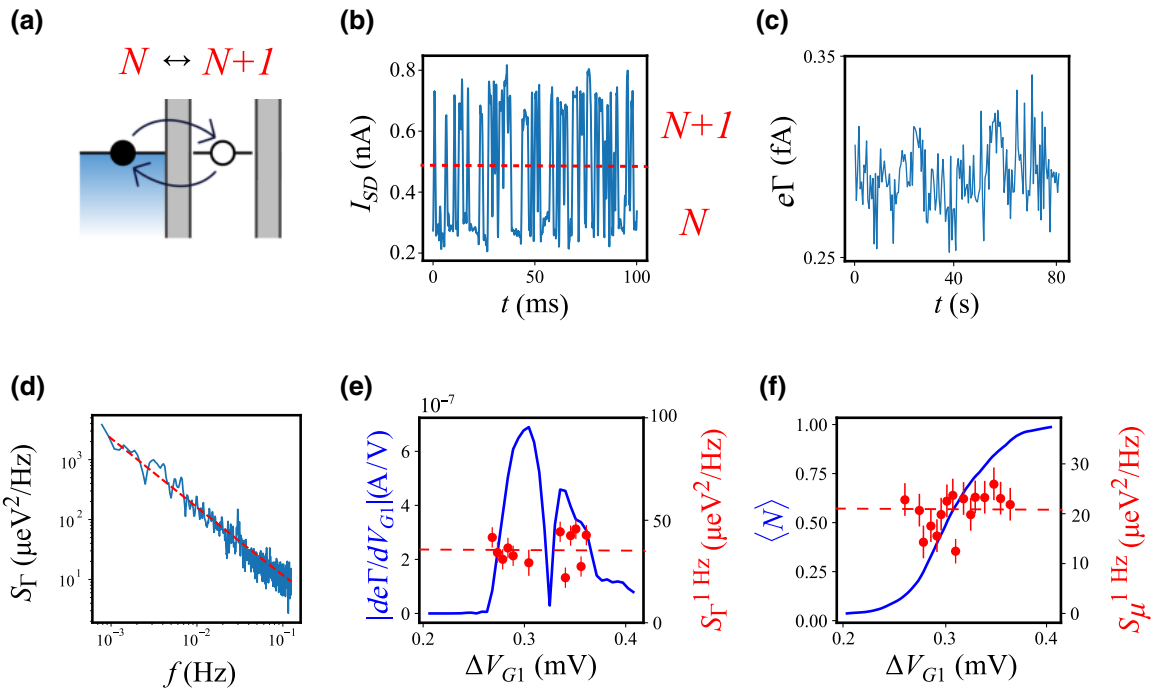

FIG. 4. Measurement method for charge noise in a few-electron quantum dot. (a) Schematic of the quantum dot configuration to be probed. The first available energy level in the quantum dot is brought into resonance with the reservoir potential. The occupancy of the dot varies between $N = 0$ and $N = 1$. (b) Current through the sensor dot measured over 100 ms. A threshold is set to distinguish the two charge states of the probed dot (c) The variation in the equivalent current $e\Gamma$ is plotted over the course of a single measurement. (d) Power spectral density obtained by Fourier transform of the plot in (c). (e) In blue, charge sensitivity of the transition. In red, variation of the renormalized PSD at 1 Hz as a function of the gate voltage for the same transition. (f) The blue curve represents the evolution of the dot occupancy as a function of gate voltage. The derivative of such curve reflects the sensitivity of the chemical potential to charge noise. The red dots correspond to charge noise acting purely on the chemical potential and are extracted from $\langle N\rangle(t)$ time traces.

quite large and related to two parameters. First the number of data samples available at low frequency is low to conduct the experiment in a reasonable time. The second reason is due to fluctuations in the charge noise across a Coulomb peak as observed in Figs. 4(e) and 4(f). This can be attributed to local fluctuations in the density of TLS as the gate is swept. Despite these error bars we can observe in Fig. 5 a clear decrease in the charge noise magnitude as the number of electrons increases in the quantum dot. There are three different mechanisms to explain this behavior. The first one is the difference in electric field for the different electron numbers. For instance, measurements in the few-electron regime require the presence of a charge detector and therefore different biasing conditions compared to the many-electron regime. The second potential explanation is a geometric consideration. As the number of electrons increases in the quantum dot, the volume of the quantum dot increases due to Coulomb interaction and modification of the confinement potential shape. It leads to an increase in distance between the charge noise source, beyond the interface, and the average electron position, decreasing their dipolar interaction. This assumes that the dominant fluctuators are located in the interface directly above the quantum dot. The observed data are supported qualitatively by simulating the effect of a single TLS above the interface on the chemical potential of the quantum dot for three different quantum dot occupations (see

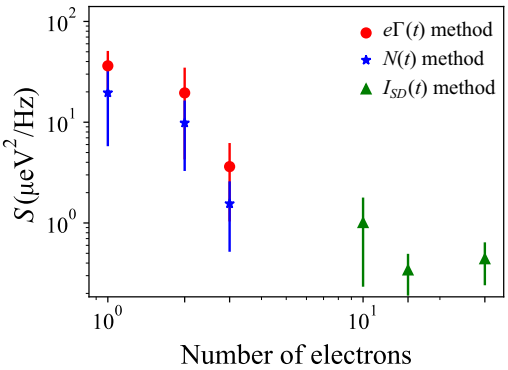

FIG. 5. Charge noise as a function of the dot occupancy. The first three points for electron numbers 1, 2, and 3 are measured using the single-shot method, deconstructed into the $e\Gamma(t)$ and $\langle N\rangle(t)$ contributions. The other points are measured in similar electrostatic configurations using the I_{SD} method on the flank of a Coulomb peak. The values quoted here are for measurements conducted at a temperature of 360 mK.

Appendix A). Finally, screening effects can appear as the electron number increases, leading to a reduction of the potential fluctuations, but this is expected to be a second-order correction [24]. It is important to note that probing charge noise in the range $N_e = 4$ to 10 is not possible with the present methods as the tunneling rate is on the one hand too low to perform I_{SD}-based measurement and on the other hand too high to use real-time tunneling analysis. One possible technique to overcome this challenge is to use rf-based reflectometry which allows probing of tunneling rate in the range of 10–1000 MHz [25].

V. CONCLUSION

In conclusion, we have shown that the charge noise obtained from current spectroscopy gives valuable information on the effect of TLS on the quantum dot chemical potential. In particular, the charge noise strongly depends on the configuration of the quantum dot which can be tuned using the different gate potentials. It also shows that the source and drain junctions are an important source of noise, which could be mitigated in future quantum technology applications via more precise control of the reservoir tunnel barriers or different choice of materials.

Finally, we have shown that characterizing charge noise in the many-electron regime is not sufficient to capture the full noise picture. We have used a method based on single-shot readout to extract the charge noise down to the single-electron level. It has allowed us to disentangle the pure chemical potential noise from the tunnel coupling fluctuations. Moreover, the method is experimentally simple to implement, requiring only charge detection of time-resolved tunneling at the single-electron level. It has allowed us to extract the charge noise susceptibility of the quantum dot as a function of electron number which shows a decrease in charge noise at higher occupancy. This last result adds to the potential benefits of operating a quantum dot in the few-electron regime to improve charge-noise-limited quantum-dot-based spin qubits [26].

ACKNOWLEDGMENT

We acknowledge technical support from P. Perrier, H. Rodenas, E. Eyraud, D. Lepoittevin, I. Pheng, T. Crozes, L. Del Rey, D. Dufeu, J. Jarreau, J. Minet, and C. Guttin. We thank Jing Li for fruitful discussions on the $1/f$ noise model. C.S., B.K, and D.J.N. acknowledge the GreQuE doctoral programs (Grant Agreement No. 754303). The device fabrication is funded through the Mosquito project (Grant Agreement No. 688539). This work is supported by the Agence Nationale de la Recherche through the CRYMCO project and the CMOSQSPIN project. This project also receives funding from the QuCube project (Grant Agreement No. 810504) and the QLSI project (Grant Agreement No. 951852).

APPENDIX A: SIMULATION OF CHARGE NOISE FOR THREE DIFFERENT ELECTRON OCCUPANCIES AS A FUNCTION OF BACK GATE VOLTAGE

We compute the energies of N-electron configurations in QD_1 in a self-consistent Schrödinger-Poisson approximation in which each electron moves in the potential created by the gates and by the mean-field density $(N-1)/N \times \rho(\mathbf{r})$, where $\rho(\mathbf{r})$ is the total electronic density and the factor $(N-1)/N$ accounts for the fact that each electron only interacts with $N-1$ others in the dot. Screening in the source and drain is accounted for in a linearized Thomas-Fermi approximation. To model the effect of a single fluctuator close to the dot, we compute the change of chemical potential when a single charge at the top interface of the channel moves by 1 nm perpendicular to the channel axis (see Fig. 6). The chemical potential fluctuations decrease when the back gate voltage is increased and the electron wave function moves from the top to the bottom interface, and when the number of electrons in the dot decrease, due to swelling of the dot (which extends further away from the charge) and to screening.

APPENDIX B: ASSESSING THE EFFECT OF VERY-LOW-FREQUENCY CHARGE FLUCTUATORS

1. Temperature dependence of charge noise

As the characteristic fluctuation frequency of TLS follows an Arrhenius law $e^{-E_\alpha/k_B T}$, temperature can provide important information on the charge noise source structure [27]. Therefore, we investigate the temperature dependence of charge noise at 1 Hz in the device. For this purpose, we sweep the temperature from 400 mK to 4

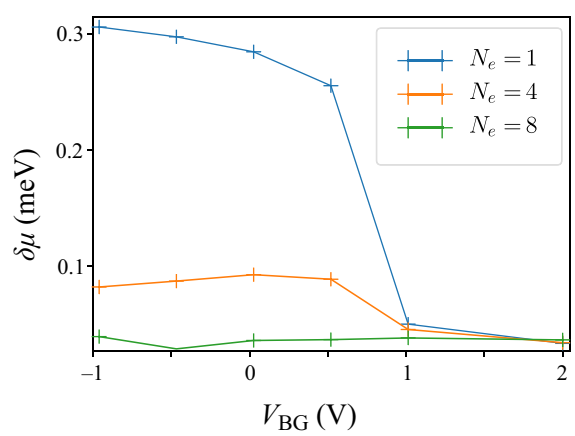

FIG. 6. Simulation of the variation of chemical potential induced by a two-level fluctuator as a function of the number of electrons in the dot and the back gate bias. It shows a qualitative agreement with the experimental variations of charge noise with both number of electrons and back gate voltage.

K. In addition, as a control experiment we measure the charge noise at two different chemical potential configurations, corresponding to 10 and 30 electrons, respectively. Figure 7(a) presents the charge noise as a function of temperature for these two cases. It shows a strong deviation from the expected linear dependence of charge noise [28]. This is a signature of a nonuniform distribution of the TLS energies. To further explore the noise structure, we investigate the gradient of the power spectrum at 1 Hz.

2. Reconstruction of TLS spectrum

Figure 7(b) presents the simulated characteristic spectra of a group of TLSs evenly coupled to the quantum dot at a fixed temperature. The green curve corresponds to the archetypal $1/f$ spectrum, which is the spectrum obtained by measuring a set of TLSs with a uniform distribution of characteristic frequencies. The purple curve shows the power spectrum for a group of TLS with a distribution of characteristic frequencies centered at relatively high frequency. The main consequence is that the gradient of the power spectrum is close to zero at 1 Hz. The last case (yellow curve) corresponds to a group of TLS with low characteristic frequency. The $1/f^2$ dependence at 1 Hz originates from the Lorentzian contribution of TLS to the power spectrum. A real spectrum consists of a combination of these signatures dependent on the distribution of TLSs in the system. Analysis of the gradient of the power spectrum at different frequencies can therefore give information about the fluctuators present in the system. In order to probe a wide range of frequencies, we vary the temperature of the system. We assume the activation energy E_α of a individual fluctuators to be fixed, and their characteristic frequency to be given by a kinetic process following an Arrhenius law e^{-E_α/k_BT} (see Appendix B 1).

To probe the distribution of activation energies of the dominant fluctuators, we systematically extract the parameter $\Gamma = \partial \ln S_\epsilon / \partial \ln f$, the gradient of the power spectrum at 1 Hz in logarithmic scale. Figure 7(c) shows the evolution of Γ as a function of temperature. From this, we can qualitatively reconstruct the full spectrum of TLSs at a given temperature based on the extracted Γ. Figure 7(d) is a simulation of the charge noise using two groups with activation energy distributions centered at 0.1 meV and 1.5 meV. One group has a high characteristic frequency, which likely corresponds to the dopants on the edge of the reservoir that dominate the increase in charge noise with top gate. The other has lower characteristic frequency, which is expected to be seen with TLSs located at the interfaces or embedded in the gate stack or buried oxide.

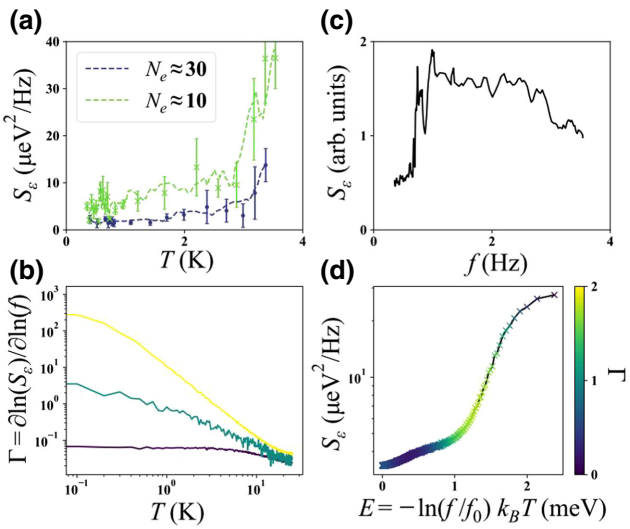

FIG. 7. (a) Power spectral density measured at 1 Hz as a function of temperature for two different dot configurations: the first visible Coulomb peak (a few-electron configuration, with $N_e \approx 10$; green), and the many-electron regime ($N_e \approx 30$; purple). V_{TG} and V_{BG} are kept constant. The number of electrons is varied by increasing the on-site potential via plunger gate V_{G1}. (b) Simulations of three different fluctuator configurations. Low-frequency dominant fluctuators are simulated at 0.1 Hz (yellow), indicating a steep $1/f^2$ shape at 1 Hz. A distribution of many fluctuators at different frequencies (linear interpolation from 0.1 Hz to 100 Hz) is simulated with equal amplitudes (green), demonstrating archetypal $1/f$ noise. High-frequency dominant fluctuators are simulated at 10 Hz (purple), demonstrating a shifted Lorentzian shape that tends towards $\partial \ln(S_\epsilon)/\partial \ln(f) = 0$ at 1 Hz. (c) The measured $\partial \ln(S_\epsilon)/\partial \ln(f)$ at 1 Hz as a function of temperature for the configuration $N_e \approx 10$. (d) Simulation of the PSD produced by two bistable fluctuators that satisfy the measured $\partial \ln(S_\epsilon)/\partial \ln(f)$ from (c). The simulated fluctuators have energies 0.1 meV and 1.5 meV. This curve gives the charge noise for any combination of f and T within the range of energy probed for this particular configuration. The color scale indicates the expected gradient of the related charge noise with frequency.

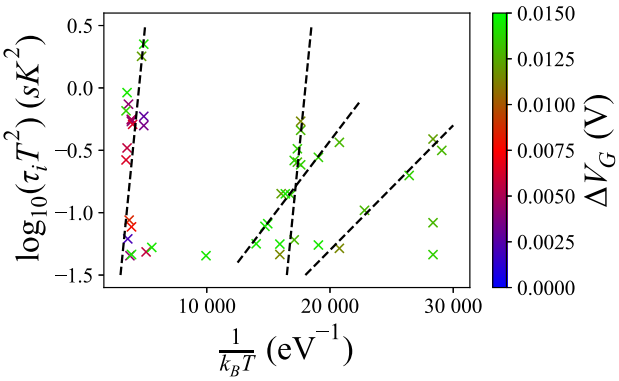

FIG. 8. Arrhenius diagram of the frequency of individual fluctuators detected in a series of charge noise measurements made over a temperature range from 0.3 K to 4 K. The color scale gives the voltage offset from a reference point at the Coulomb peak for each detected dominating fluctuator. Points which are caused by the same fluctuator are expected to have approximately the same voltage offset.

3. Arrhenius activation energy for identified TLS

An Arrhenius plot was used to confirm the individual fluctuator energies extracted using the energetic simulation, and to obtain their energies independent of the characteristic frequency. For a single-quantum-dot configuration, charge noise measurements were taken over a temperature range from 0.3 K to 4 K. The time constant of these dominant fluctuators was determined by fitting the noise spectrum with a Gaussian expression and extracting the central frequency. The time constant was then plotted against the temperature (Fig. 8). Two groups of fluctuators were observed to change linearly with temperature. The energy of these fluctuators was determined by their gradient, giving 0.15 meV and 1.35 meV respectively, in good agreement with the values obtained through simulation.

[1] B. E. Kane, A silicon-based nuclear spin quantum computer, Nature **393**, 133 (1998).

[2] J. T. Muhonen, J. P. Dehollain, A. Laucht, E. F. Hudson, R. Kalra, T. Sekiguchi, K. M. Itoh, D. N. Jamieson, J. C. McCallum, A. S. Dzurak, and A. Morello, Storing quantum information for 30 seconds in a nanoelectronic device, Nat. Nanotechnol. **9**, 986 (2014).

[3] J. Yoneda, K. Takeda, T. Otsuka, T. Nakajima, M. Delbecq, G. Allison, T. Honda, T. Kodera, S. Oda, Y. Hoshi, *et al.*, A quantum-dot spin qubit with coherence limited by charge noise and fidelity higher than 99.9%, Nat. Nanotechnol. **13**, 102 (2018).

[4] A. Noiri, K. Takeda, T. Nakajima, T. Kobayashi, A. Sammak, G. Scappucci, and S. Taruch, Fast universal quantum gate above the fault-tolerance threshold in silicon, Nature **601**, 7893 (2022).

[5] D. Culcer, X. Hu, and S. Das Sarma, Dephasing of Si spin qubits due to charge noise, Appl. Phys. Lett. **95**, 073102 (2009).

[6] E. J. Connors, J. J. Nelson, H. Qiao, L. F. Edge, and J. M. Nichol, Low-frequency charge noise in Si/SiGe quantum dots, Phys. Rev. B **100**, 165305 (2019).

[7] E. Chanrion, D. J. Niegemann, B. Bertrand, C. Spence, B. Jadot, J. Li, P.-A. Mortemousque, L. Hutin, R. Maurand, X. Jehl, M. Sanquer, S. De Franceschi, C. Bäuerle, F. Balestro, Y.-M. Niquet, M. Vinet, T. Meunier, and M. Urdampilleta, Charge Detection in an Array of CMOS Quantum Dots, Phys. Rev. Appl. **14**, 024066 (2020).

[8] M. Urdampilleta, D. J. Niegemann, E. Chanrion, B. Jadot, C. Spence, P.-A. Mortemousque, C. Bäuerle, L. Hutin, B. Bertrand, S. Barraud, R. Maurand, M. Sanquer, X. Jehl, S. DeFranceschi, M. Vinet, and T. Meunier, Gate-based high fidelity spin readout in a CMOS device, Nat. Nanotechnol. **14**, 737 (2019).

[9] V. N. Ciriano-Tejel, M. A. Fogarty, S. Schaal, L. Hutin, B. Bertrand, L. Ibberson, M. F. Gonzalez-Zalba, J. Li, Y.-M. Niquet, M. Vinet, and J. J. L. Morton, Spin Readout of a CMOS Quantum Dot by Gate Reflectometry and Spin-Dependent Tunnelling, PRX Quantum **2**, 010353 (2021).

[10] A. West, B. Hensen, A. Jouan, T. Tanttu, C. H. Yang, A. Rossi, M. F. Gonzalez-Zalba, F. E. Hudson, A. Morello, D. J. Reilly, and A. S. Dzurak, Gate-based single-shot readout of spins in silicon, Nat. Nanotechnol. **14**, 437 (2019).

[11] R. Maurand, X. Jehl, D. Kotekar-Patil, A. Corna, H. Bohslavskyi, R. Laviéville, L. Hutin, S. Barraud, M. Vinet, M. Sanquer, and S. De Franceschi, A CMOS silicon spin qubit, Nat. Commun. **7**, 13575 (2016).

[12] A. Crippa, R. Ezzouch, A. Aprá, A. Amisse, R. Laviéville, L. Hutin, B. Bertrand, M. Vinet, M. Urdampilleta, T. Meunier, M. Sanquer, X. Jehl, R. Maurand, and S. De Franceschi, Gate-reflectometry dispersive readout and coherent control of a spin qubit in silicon, Nat. Commun. **10**, 2776 (2019).

[13] J. P. Kestner, X. Wang, L. S. Bishop, E. Barnes, and S. Das Sarma, Noise-Resistant Control for a Spin-Qubit Array, Phys. Rev. Lett. **110**, 140502 (2013).

[14] T. Struck, A. Hollmann, F. Schauer, O. Fedorets, A. Schmidbauer, K. Sawano, H. Riemann, N. V. Abrosimov, L. Cywiński, D. Bougeard, and L. R. Schreiber, Low-frequency spin qubit energy splitting noise in highly purified ^{28}Si/SiGe, npj Quantum Inf. **6**, 1 (2020).

[15] E. J. Connors, J. J. Nelson, and J. M. Nicho, Charge-noise spectroscopy of Si/SiGe quantum dots via dynamically-decoupled exchange oscillations, Nat. Commun. **13**, 1 (2022).

[16] M. Vinet, L. Hutin, B. Bertrand, S. Barraud, J-M. Hartmann, Y-J. Kim, V. Mazzocchi, A. Amisse, H. Bohuslavskyi, L. Bourdet, *et al.*, in *2018 IEEE International Electron Devices Meeting (IEDM)* (IEEE, San Francisco, CA, USA, 2018), p. 6.

[17] R. M. Jock, N. T. Jacobson, P. Harvey-Collard, A. M. Mounce, V. Srinivasa, D. R. Ward, J. Anderson, R. Manginell, J. R. Wendt, M. Rudolph, T. Pluym, J. K. Gamble, A. D. Baczewski, W. M. Witzel, and M. S. Carroll, A silicon metal-oxide-semiconductor electron spin-orbit qubit, Nat. Commun. **9**, 1 (2018).

[18] X. Mi, S. Kohler, and J. R. Petta, Landau-Zener interferometry of valley-orbit states in Si/SiGe double quantum dots, Phys. Rev. B **98**, 161404 (2018).

[19] J.-S. Kim, T. M. Hazard, A. A. Houck, and S. A. Lyon, A low-disorder metal-oxide-silicon double quantum dot, Appl. Phys. Lett. **114**, 043501 (2019).

[20] J. You, H.-O. Li, K. Wang, G. Cao, X.-X. Song, M. Xiao, and G.-P. Guo, Suppression of low-frequency charge noise in gates-defined GaAs quantum dots, Appl. Phys. Lett. **107**, 233104 (2015).

[21] J. Kamioka, T. Kodera, K. Takeda, T. Obata, S. Tarucha, and S. Oda, Charge noise analysis of metal oxide semiconductor dual-gate Si/SiGe quantum point contacts, J. Appl. Phys. **115**, 203709 (2014).

[22] J.-S. Kim, A. M. Tyryshkin, and S. A. Lyon, Annealing shallow Si/SiO_2 interface traps in electron-beam irradiated high-mobility metal-oxide-silicon transistors, Appl. Phys. Lett. **110**, 123505 (2017).

[23] B. M. Freeman, J. S. Schoenfield, and H. Jiang, Comparison of low frequency charge noise in identically patterned Si/SiO2 and Si/SiGe quantum dots, Appl. Phys. Lett. **108**, 253108 (2016).

[24] E. Barnes, J. P. Kestner, N. T. T. Nguyen, and S. Das Sarma, Screening of charged impurities with multi-electron singlet-triplet spin qubits in quantum dots, Phys. Rev. B **84**, 235309 (2011).

[25] M. G. House, T. Kobayashi, B. Weber, S. J. Hile, T. F. Watson, J. van der Heijden, S. Rogge, and M. Y. Simmon, Radio frequency measurements of tunnel couplings and singlet–triplet spin states in Si:P quantum dots, Nat. Commun. **6**, 8848 (2015).

[26] R. C. C. Leon, C. H. Yang, J. C. C. Hwang, J. C. Lemyre, T. Tanttu, W. Huang, K. W. Chan, K. Y. Tan, F. E. Hudson, K. M. Itoh, A. Morello, A. Laucht, M. Pioro-Ladriére, A. Saraiva, and A. S. Dzurak, Coherent spin control of s-, p-, d- and f-electrons in a silicon quantum dot, Nat. Commun. **11**, 1 (2020).

[27] S. Ahn, S. Das Sarma, and J. P. Kestner, Microscopic bath effects on noise spectra in semiconductor quantum dot qubits, Phys. Rev. B **103**, L041304 (2021).

[28] L. Petit, J. M. Boter, H. G. J. Eenink, G. Droulers, M. L. V. Tagliaferri, R. Li, D. P. Franke, K. J. Singh, J. S. Clarke, R. N. Schouten, V. V. Dobrovitski, L. M. K. Vandersypen, and M. Veldhors, Spin Lifetime and Charge Noise in Hot Silicon Quantum Dot Qubits, Phys. Rev. Lett. **121**, 076801 (2018).